Magnetic properties of iron nanoparticle

6 authors, including:

Jeff Carvell
Indiana University-Purdue University Indianapolis
10 PUBLICATIONS   **79** CITATIONS

Elijah Ayieta
University of Nairobi
15 PUBLICATIONS   **75** CITATIONS

Andrew Gavrin
Indiana University-Purdue University Indianapolis
65 PUBLICATIONS   **2,789** CITATIONS

Ruihua Cheng
Indiana University-Purdue University Indianapolis
27 PUBLICATIONS   **263** CITATIONS

Some of the authors of this publication are also working on these related projects:

Project   KSU LT Doctorial Research View project

Project   SANS project View project

Magnetic properties of iron nanoparticle

J. Carvell,[1] E. Ayieta,[1] A. Gavrin,[1] Ruihua Cheng,[1,a)] V. R. Shah,[2,b)] and P. Sokol[2]

[1]*Department of Physics, Indiana University Purdue University Indianapolis, 402 N Blackford Street Indianapolis, Indiana 46202, USA*
[2]*Department of Physics, Indiana University, 727 E. Third Street Bloomington, Indiana 47405, USA*

Magnetic properties of Fe nanoparticles with different sizes synthesized by a physical deposition technique have been investigated experimentally. We have used a high pressure sputtering technique to deposit iron nanoparticles on a silicon substrate. The nanoparticles are then analyzed using atomic force microscopy (AFM), transmission electron microscopy (TEM), and superconducting quantum interference device techniques. TEM and AFM data show that the particle size could be tuned by adjusting the deposition conditions. The magnetic properties have been investigated from temperature dependent magnetization $M(T)$ and field dependent magnetization $M(H)$ measurements. The results show that two phases including both ferromagnetic and superparamagnetic particles are present in our system. From these data we extracted the superparamagnetic critical size to be 9 nm for our samples. Ferromagnetic particles are single magnetic domain particles and the magnetic properties can be explained by the Stoner and Wohlfarth model. For the superparamagnetic phase, the effective anisotropy constant, K_{eff}, decreases as the particle size increases. © *2010 American Institute of Physics.* [doi:10.1063/1.3428415]

I. INTRODUCTION

The properties of magnetic nanoparticles have been explored widely in the last decades due to the large number of applications in the areas of spintronics, biology, and medical science.[1–4] Magnetic nanoparticles are an important class of nanostructured materials offering high potential as high density data storage media,[5,6] magnetic targeting drug delivery, high resolution magnetic resonance imaging, and hyperthermia generation agents.[7,8] Compared with bulk structures, whose properties are well known, magnetic nanoparticles are complex and manifest a great diversity in their properties because the energies associated with the various physical parameters are comparable in the nanostructures. These parameters include the magnetocrystalline anisotropy energy,[9] surface anisotropy energy,[10,11] and thermal energy. The magnetic properties of nanoparticles are very sensitive to the composition, structure, size, and local environment. There are a number of key issues that need to be explored. Among them are (i) the problem of finite size scaling: there is a drop in the magnetic Curie temperature with decreasing size of a magnetic system, and (ii) the superparamagnetic limit: the size limit where thermal fluctuations flip the magnetization of an individual "nanoparticle" on a time scale so short that an array of such magnetic particles is paramagnetic.[12] The desired properties for each of these applications are not necessarily the same. The creation and a comprehensive understanding of magnetic nanoparticles are crucial in order to meet the needs of the applications in various fields.

Different approaches, including chemical synthesis and vapor deposition, are reported in the literature for nanoparticles fabrication.[13–19] In our experiment, iron nanoparticles were fabricated using a high pressure magnetron sputtering technique.

Previous experiments have shown that controlling the deposition conditions of a modified high pressure sputtering technique would allow for the tuning of the size of iron nanoparticles. In this work, iron nanoparticles ranging in size from 15–30 nm were fabricated. Transmission electron microscopy (TEM) and atomic force microscopy (AFM) results indicate that different sized particles can be created with well controlled experimental conditions. Diffraction data on the sample show that the particles adopt a body-centered cubic structure. Magnetic measurements taken using a superconducting quantum interference device (SQUID) show that two phases, including both ferromagnetic and superparamagnetic, occur in our system. For the ferromagnetic phase, Fe particles show single domain magnetic structure as the coercivity of the nanoparticles increases with the particle size increases. The data allow for the magnetic anisotropy constant to be derived. For the superparamagnetic phase, a magnetization as a function of temperature study showed that the blocking transition temperature of the nanoparticles also increases as the particle size increases.

II. EXPERIMENTAL METHODS

The Fe nanoparticles were prepared on Si (100) substrates with a high pressure sputtering system. This system is composed primarily of a source gun and a deposition chamber. It is a combination of magnetron sputtering and gas aggregation techniques. In this method, argon gas was introduced inside the sputtering gun. The gun is equipped with a nozzle that raises the gas pressure near the target surface. Cluster formation occurs because the atomic mean free paths

a)Electronic mail: rucheng@iupui.edu.
b)Present address: Nebraska Center for Materials and Nanoscience, University of Nebraska-Lincoln, Lincoln, NE 68588, USA.

(a)   (b)

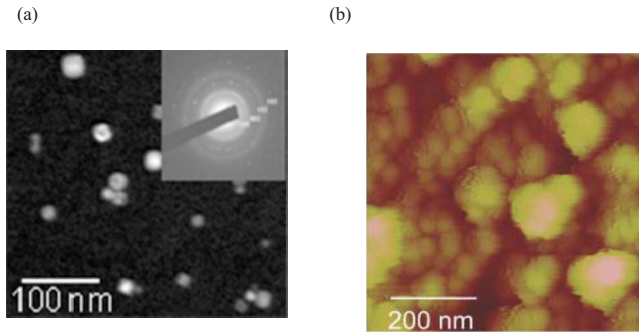
FIG. 1. (Color online) (a) TEM and (b) AFM images of Fe nanoparticles. The inset shows the selective area diffraction pattern obtained from HRTEM.

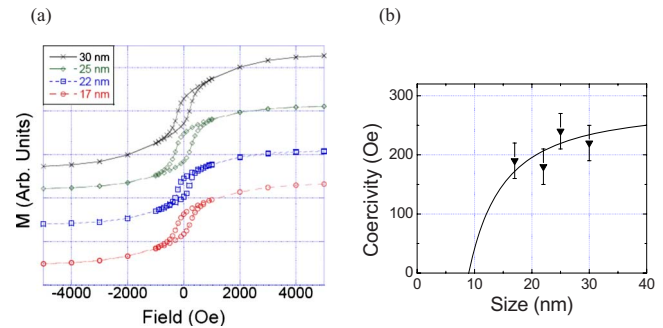(a)   (b)

FIG. 2. (Color online) (a) Magnetization curves measured at 300 K for various sample sizes. (b) The coercivity plotted as a function of particle size. The solid line is the fitting according to the single domain Stoner and Wohlfarth model.

decrease due to the large Ar gas pressure inside the gun. The nozzle used in this experiment had a diameter of 0.1 in. and a length of 1.5 in.

The high pressure of the argon gas inside the nozzle also results in a large pressure difference between the source gun and the deposition chamber outside the nozzle. The particles are produced in a small volume above the target surface in the source gun and the pressure difference between the gun and the deposition chamber allows the clusters to enter the deposition chamber, where they are deposited on a substrate. The base pressure of the vacuum chamber was about 5 $\times 10^{-8}$ Torr. We used a mass flow controller to control the amount of argon gas that was introduced into the sputtering gun. The gas pressure both inside the gun and inside the chamber was monitored through gauges. Fe nanoparticles of variable mean size from 15–30 nm are produced under different gun pressures. As the flow rate increases, the gun pressure increases as well. The cluster size is controlled by changing the flow rate of the Ar gas. The sputtering power was kept at 50 W for each case. The effective growth rate was calibrated by using a quartz single crystal thickness monitor.

Analysis of the samples was done using several techniques. TEM and AFM imaging were done to verify the size distribution of the fabricated nanoparticles. Selected area diffraction was used to verify the structure of the iron. We also performed x-ray diffraction (XRD) measurements using a Siemens D-5000 diffractometer (Cu *K*a radiation) in order to obtain information on the structure of the nanoparticles. SQUID measurements were obtained to study the magnetic properties of the nanoparticles. Hysteresis loops were obtained both at room temperature and at low temperature (5 K) for various samples. The magnetization was measured as the applied magnetic field was varied from $-50\,000$ to 50 000 Oe (-5 to 5 T). Magnetization versus temperature graphs were recorded both with field cooling (FC) and zero-field cooling (ZFC). In this case, the magnetization of the samples was measured over a temperature range of 5–390 K, with a constant 100 Oe field applied.

III. RESULTS AND DISCUSSION

The morphology and size distribution of the particles created under different gun pressures were studied using TEM and tapping mode AFM imaging. Figure 1 shows the

TEM and AFM images of the iron nanoparticles. Larger clusters seen in the image are the result of aggregation of several particles. Data show that the size of the particles depends on the deposition conditions. Increasing the Ar gas pressure inside the source gun leads to an increase in the size of the particles because the atom mean free path decreases as the pressure increases. The mean particle size could be easily tuned by changing the deposition conditions. A selective area diffraction pattern, shown in the inset of Fig. 1 obtained from the TEM verified that the structure was body-centered cubic with a lattice spacing 0.286 nm. The circles in the pattern, obtained from a large sample area, indicate the clusters are polycrystalline. The high resolution TEM results indicate that the Fe nanoclusters were covered uniformly with iron oxide shells composed of very small nanocrystallites. This is because the zero-valence iron exposed to air or any oxygen-including atmosphere is oxidized readily. The iron oxide shell has a thickness of about 1–2 nm independent of the nanoparticle size. We observed that the core-shell nanoclusters are very stable against further oxidation after a long time exposure to air.

Data obtained from the SQUID measurements were used to study the magnetic properties of the samples. Figure 2(a) shows the normalized magnetization, *M*, as a function of the applied magnetic field for several samples with different sizes of nanoparticles at room temperature. We have observed a clear ferromagnetic signal given that the $M(H)$ curves show hysteresis. From these graphs, the coercivity for each of the samples with different particle sizes was obtained. The mean size of the particles was calibrated by TEM and AFM as described in the previous paragraph. Figure 2(b) shows the coercivity as a function of mean particle size at room temperature. It clearly shows a trend that as the particle size increases, the coercivity of the sample increases as well. When the measurements were taken, some background from the substrate contributed to the measurements, and these background signals were subtracted before the data analysis. The corresponding coercivities do show a dependence on the size of the nanoparticles. The coercivities measured for each of samples are symmetric with respect to the magnetic fields.

The fact that the coercivity of the nanoparticles increases as the size increases can be explained by the Stoner and Wohlfarth model. If the particles were relatively large they

TABLE I. Magnetic characteristics of various samples derived from magnetic measurements and modeling.

Sample	Ferromagnetic phase size (nm)	H_C (Oe)	K_u (MJ/m^3)	Superparamagnetic phase size (nm)	T_B (K)	K_{eff} (MJ/m^3)
1	17	210	0.18	3.8	113	1.39
2	22	178	0.16	4.8	124	0.76
3	25	250	0.21	5.9	121	0.41
4	30	200	0.17	7.9	130	0.27

would be multidomain and the mechanism of magnetization reversal would be domain wall nucleation and motion. In that case the coercivity would decrease with increasing size. However, for small particles, the energy of the domain wall dominates and single domain particles are stable below a critical size and the magnetization reversal would occur with magnetization rotation as described by the Stoner and Wohlfarth model. The coercivity follows the relationship,[20] $H_C = 2K_u/M_S$, where K_u is the uniaxial anisotropy constant. The magnetic anisotropy for a cubic structure is relatively weak. Because we find increasing H_C with increasing size, we conclude that our particles are single domain magnets with a uniaxial magnetic anisotropy since no crystalline orientation is favored and the anisotropy axes of the particles are randomly oriented in our samples. K_u is estimated to be ~0.20 MJ/m^3, as listed in Table I for various sized samples, and K_u increases with decreasing particle size. Taking account of thermal fluctuations in the single domain Stoner and Wohlfarth model, the coercivity approximately depends on the particle size as a function of $H_C(d) = 0.5H_k[1 - (d_p/d)^{3/2}]$, where H_k is the anisotropy field and d_p is the superparamagnetic particle size. Hence the superparamagnetic particle size can be extracted from the magnetic hysteresis loops of samples with different mean particle size. The data fitting of H_C in our samples, shown as the solid line in Fig. 2(b), results in d_p to be 9 nm.

The magnetization as a function of the applied field was also obtained for the case when the temperature was held constant at 5 K. Figure 3(a) shows the hysteresis curves taken at 5 K for the various samples with different nanoparticle size, and Fig. 3(b) shows the coercivity approaching from positive and negative saturation, as a function of the nanoparticle size. Overall it can be seen in the hysteresis measurements that the coercivity for particular nanoparticle sizes is higher at 5 K than at room temperature as expected for ferromagnetic materials. The shape of the hysteresis loops obtained both at room temperature and low temperature shows a deviation from the Stoner–Wohlfarth model. This could be due to the surface anisotropy of the particles and magnetic core shell structure results in the nonuniform reversal of the particle's magnetization.[21] We noticed that at low temperature, the coercivity when approached from positive saturation was significantly different than the coercivity measured by approaching from negative saturation. The hysteresis loops obtained at 5 K are shifted to the left with unsymmetrical coercivity. Fine hematite (α-Fe$_2$O$_3$) is known to be antiferromagnetic under the Morin transition, $T_M = 250$ K.[22] We therefore further conclude that the observed

shift of the hysteresis loops at low temperature is due to the exchange bias between antiferromagnetic α-Fe$_2$O$_3$ shell and the Fe core.

To account for the interparticle interactions, we consider that nanoparticles in close proximity are exchange coupled and those at large distances are magnetostatically coupled. For an exchange coupled system the hysteresis loop is square. The nature of the coupling can be quantitatively extracted from the ratio of remanence M_r to saturation magnetization M_S. A ratio greater than 0.5 indicates the presence of exchange coupling and a ratio less than 0.5 indicates the presence of magnetostatic coupling. Our data show the ratio to be around 0.3 indicating weak interactions between particles, most likely due to the shell layer oxidation.

The magnetization was also measured as a function of temperature for various samples. First, the nanoparticle samples were cooled from room temperature to 5 K, with zero field and a 100 Oe field was applied. The magnetization subsequently was measured over the temperature range of
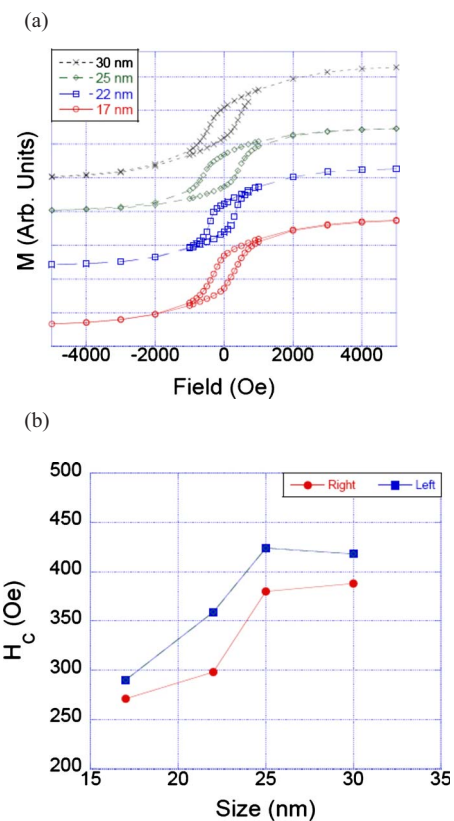

FIG. 3. (Color online) (a) Magnetization curves measured at 5 K for various sample size. (b) The coercivity plotted as a function of particle size.
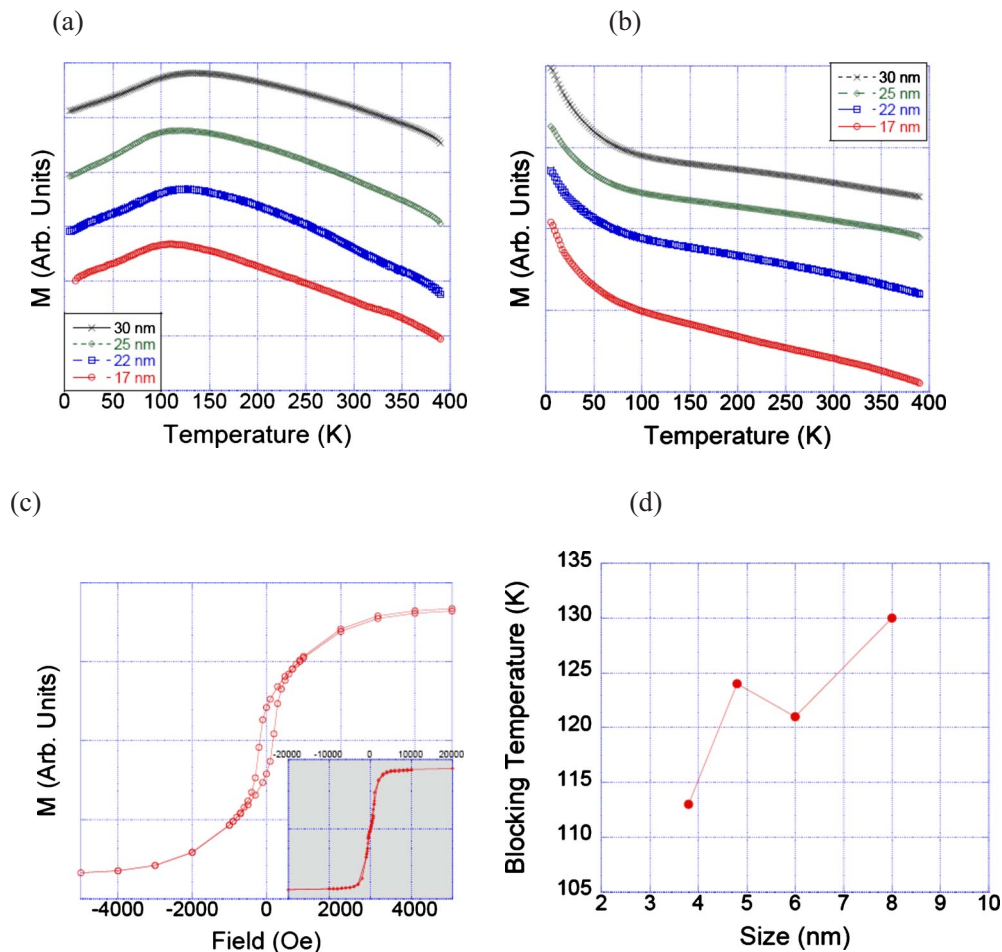
FIG. 4. (Color online) (a) ZFC and (b) FC curves measured for different samples at 5–390 K. The curves were recorded in a small magnetic field of 10 mT. (c) Magnetization curves measured at 300 K for sample with nominal size of 30 nm. The inset shows the magnetic curve of the superparamagnetic phase of the sample. (d) The maximum temperature extracted from ZFC data plotted as a function of the particle size for the superparamagnetic phase.

5–390 K, with a temperature sweep rate of around a few millidegrees kelvin per second. Figure 4(a) shows the so-called ZFC results obtained from these measurements. It can be seen from these plots that the magnetization of the sample increases to a maximum value before it starts going down again. The temperature peak in a ZFC $M(T)$ curve is the typical feature of superparamagnetic behavior and the temperature where this maximum value occurs, T_{max}, is the blocking temperature, T_B, where the transition from ferromagnetic to superparamagnetic takes place.

The measurements were repeated with the field applied as the temperature was lowered from room temperature to 5 K following the FC protocol. Figure 4(b) shows the FC $M(T)$ curves for various samples. The peaks exhibited in the ZFC data are not expected for pure ferromagnetic materials. The ZFC and FC data suggest a superparamagnetic phase. This indicates that a dual phase including ferromagnetic and superparamagnetic particles is present in our samples. This phenomenon can be explained by the fact that aggregation of small superparamagnetic particles forms ferromagnetic particles. When the $T > T_{max}$, $M(T)$ curves show a deviation from a $1/T$ behavior, this suggests a dual phase-including both ferromagnetic and superparamagnetic particles. We have decomposed the hysteresis curves taken at 300 K for samples with different particle size into two components

with contributions from ferromagnetic and superparamagnetic phases separately as shown in Fig. 4(c).

The behavior of superparamagnetic noninteracting particles can be described by the Langevin function $M(H,T) = M_S L[mH/k_B T]$, where $M(H,T)$ is the magnetization at temperature T and field H, M_S is the saturation magnetization, L is the Langevin function $L(x) = \coth(x) - 1/x$, and $m = M_S(\pi d^3/6)$ is the magnetic moment of a sphere. The average superparamagnetic-particle diameter can be obtained by fitting the slope of the magnetization near zero field regions $(dM/dH)_{H=0}$ at 300 K. The average particle diameter is estimated by using the following relation,[23] $d = (18k_B T(dM/dH)_{H=0}/\pi\rho M_S^2)^{1/3}$, where ρ is the density. The slope, $(dM/dH)_{H=0}$ at 300 K, of each sample is obtained by separating the contribution from the superparamagnetic phase. The average size of the superparamagnetic phase in various samples with different nominal particles size is estimated from the data fitting according to above equation. The results of the fitting are summarized in Table I, and the size of superparamagnetic phase particles is around 4–8 nm. The accepted saturation magnetization M_S of Fe is 1707 emu/cm^3 at ambient conditions.[24]

As it can be seen in Fig. 4(a), the maximum temperature, T_{max}, increases as the nanoparticle size increases and it is

plotted in Fig. 4(d) as a function of the particle size of the superparamagnetic phase. For superparamagnetic particles, if the thermal energy $k_B T$ is comparable with the energy barrier of the superparamagnetic states, the magnetization can be easily reversed and the switching can be described by Arrhenius–Néel equation, $f = f_0 e^{-(K_{\text{eff}} V / k_B T)t}$, where K_{eff} is the effective anisotropy constant of the superparamagnetic material, f is the frequency of switching, and f_0 is a constant equal to 10^9 s^{-1}. The requirement for stability of the magnetic state is $K_{\text{eff}} V > 25 k_B T$, and $K_{\text{eff}} V = 25 k_B T_B$ generally is used to derive the anisotropy constant. The effective anisotropy constants, K_{eff}, of the superparamagnetic phase for various samples are extracted and listed in Table I. We notice that K_{eff} decreases as the particle size increases. The larger anisotropy in the small particles is due to the surface anisotropy which becomes relatively more important in the smaller particles.

IV. CONCLUSION

In conclusion, iron nanoparticles were fabricated using a high pressure sputtering technique and their size could be tuned with various deposition conditions. SQUID analysis showed that superparamagnetic and ferromagnetic phases are present in our system. Ferromagnetic particles are single magnetic domain particles and the magnetic properties can be explained by the Stoner and Wohlfarth model. We derived that the superparamagnetic critical size is 9 nm in our samples. The effective anisotropy constant for superparamagnetic phase, K_{eff}, decreases as the particle size increases.

ACKNOWLEDGMENTS

[1]S. D. Bader, Rev. Mod. Phys. **78**, 1 (2006).
[2]D. Sander, J. Phys.: Condens. Matter **16**, R603 (2004).
[3]S. Rohart, C. Raufast, L. Favre, E. Bernstein, E. Bonet, and V. Dupuis, Phys. Rev. B **74**, 104408 (2006).
[4]C. Antoniak, J. Lindner, M. Spasova, D. Sudfeld, M. Acet, M. Farle, K. Fauth, U. Wiedwald, H.-G. Boyen, P. Ziemann, F. Wilhelm, A. Rogalev, and S. Sun, Phys. Rev. Lett. **97**, 117201 (2006).
[5]S. H. Sun, C. B. Murray, D. Weller, L. Folks, and A. Moser, Science **2000**, 287 (1989).
[6]H. Zeng, J. Li, J. P. Liu, Z. L. Wang, and S. H. Sun, Nature (London) **420**, 395 (2002).
[7]Q. A. Pankhurst, N. K. T. Thanh, and S. K. Jones, J. Phys. D: Appl. Phys. **42**, 224001 (2009).
[8]C. L. Dennis, A. J. Jackson, and J. A. Borchers, Nanotechnology **20**, 395103 (2009).
[9]J. Sánchez-Barriga, M. Lucas, and F. Radu, Phys. Rev. B **80**, 184424 (2009).
[10]L. Berger, Y. Labaye, M. Tamine, and J. M. Coey, Phys. Rev. B **77**, 104431 (2008).
[11]S. Rusponi, T. Cren, N. Weiss, M. Epple, P. Buluschek, L. Claude, and H. Brune, Nature Mater. **2**, 546 (2003).
[12]D. Weller and A. Moser, IEEE Trans. Magn. **35**, 4423 (1999).
[13]Y. Shiratsuchi and M. Yamamoto, Phys. Rev. B **76**, 144432 (2007).
[14]L. Guo, Q. Huang, X. Li, and S. Yang, Phys. Chem. Chem. Phys. **3**, 1661 (2001).
[15]E. Carpenter, J. Sims, J. Wiemann, W. Zhou, and C. O'Connor, J. Appl. Phys. **87**, 5615 (2000).
[16]F. Li, C. Vipulanandan, and K. Mohanty, Colloids Surf., A **223**, 103 (2003).
[17]Y. Qiang, J. Antony, A. Sharma, J. Nutting, D. Sikes, and D. Meyer, J. Nanopart. Res. **8**, 489 (2006).
[18]P. Shah and A. Gavrin. J. Appl. Phys. **99**, 08H305 (2006).
[19]P. Shah and A. Gavrin, J. Magn. Magn. Mater. **301**, 118 (2006).
[20]E. C. Stoner and E. P. Wohlfarth, Philos. Trans. R. Soc. London, Ser. A **240**, 599 (1948).
[21]H. Kachkachi and M. Dimian, Phys. Rev. B **66**, 174419 (2002).
[22]I. Dzyaloshinsky, J. Phys. Chem. Solids **4**, 241 (1958); T. Moriya, Phys. Rev. **120**, 91 (1960).
[23]M. Chastellain, A. Petri, A. Gupta, K. V. Rao, and H. Hofmann, Adv. Eng. Mater. **6**, 235 (2004).
[24]R. Lawrence Comstock, *Introduction to Magnetism and Magnetic Recording* (Wiley, New York, 1999).